


Ultrafast electron localization in the $\text{EuNi}_2(\text{Si}_{0.21}\text{Ge}_{0.79})_2$ correlated metal

Journal Article

Author(s):

Mardegan, José R.L.; Zerdane, Serhane; Mancini, Giulia; Esposito, Vincent; Rouxel, Jérémy R.; Mankowsky, Roman; Svetina, Cristian; Gurung, Namrata; Parchenko, Sergii; Porer, Michael; Burganov, Bulat; Deng, Yunpei; Beaud, Paul; Ingold, Gerhard; Pedrini, Bill; Arrell, Christopher; Erny, Christian; Dax, Andreas; Lemke, Henrik; Decker, Martin; [Ortiz Hernández, Nazaret](#) ; Milne, Chris; Smolentsev, Grigory; Maurel, Laura; Johnson, Steven L.; Mitsuda, Akihiro; Wada, Hirofumi; Yokoyama, Yuichi; Wadati, Hiroki; Staub, Urs

Publication date:

2021-09-03

Permanent link:

<https://doi.org/10.3929/ethz-b-000505405>

Rights / license:

[Creative Commons Attribution 4.0 International](#)

Originally published in:

Physical Review Research 3(3), <https://doi.org/10.1103/PhysRevResearch.3.033211>

Funding acknowledgement:

NCCR MUST (183615) - NCCR MUST Verteilfonds (SNF)

Ultrafast electron localization in the $\text{EuNi}_2(\text{Si}_{0.21}\text{Ge}_{0.79})_2$ correlated metal

Jose R. L. Mardegan,^{1,2,*} Serhane Zerdane,^{3,*} Giulia Mancini,^{3,4} Vincent Esposito,³ Jérémy R. Rouxel,^{4,5} Roman Mankowsky,³ Cristian Svetina,³ Namrata Gurung,⁶ Sergii Parchenko,¹ Michael Porer,¹ Bulat Burganov,⁷ Yunpei Deng,³ Paul Beaud,³ Gerhard Ingold,³ Bill Pedrini,³ Christopher Arrell,³ Christian Erny,³ Andreas Dax,³ Henrik Lemke,³ Martin Decker,¹ Nazaret Ortiz,¹ Chris Milne,³ Grigory Smolentsev,⁸ Laura Maurel,⁶ Steven L. Johnson,⁷ Akihiro Mitsuda,⁹ Hirofumi Wada,⁹ Yuichi Yokoyama,¹⁰ Hiroki Wadati,^{10,11} and Urs Staub^{1,†}

¹Swiss Light Source, Paul Scherrer Institute, CH-5232 Villigen PSI, Switzerland

²Deutsches Elektronen-Synchrotron DESY, Notkestraße 85, 22607, Hamburg, Germany

³SwissFEL, Paul Scherrer Institute, CH-5232 Villigen PSI, Switzerland

⁴Laboratoire de Spectroscopie Ultrarapide (LSU) and Lausanne Centre for Ultrafast Science (LACUS), Ecole Polytechnique Fédérale de Lausanne (EPFL), ISIC-FSB, Station 6, 1015 Lausanne, Switzerland

⁵Univ Lyon, UJM-Saint-Etienne, CNRS, Graduate School Optics Institute, Laboratoire Hubert Curien UMR 5516, Saint-Etienne F-42023, France

⁶Laboratory for Multiscale Materials Experiments, Paul Scherrer Institute, CH-5232 Villigen PSI, Switzerland and Laboratory for Mesoscopic Systems, Department of Materials, ETH Zürich, 8093 Zürich, Switzerland

⁷Institute for Quantum Electronics, ETH Zürich, 8093 Zürich, Switzerland

⁸Paul Scherrer Institute, CH-5232 Villigen PSI, Switzerland

⁹Department of Physics, Kyushu University, Fukuoka 819-0395, Japan

¹⁰Institute for Solid State Physics, University of Tokyo, Chiba 277-8581, Japan and Department of Physics, University of Tokyo, Tokyo 113-0033, Japan

¹¹Graduate School of Material Science, University of Hyogo, 3-2-1, Koto, Kamigori-cho, Ako-gun, Hyogo 678-1297, Japan



(Received 27 July 2020; revised 14 May 2021; accepted 8 July 2021; published 3 September 2021)

Ultrafast electron delocalization induced by a femtosecond laser pulse is a well-known process in which electrons are ejected from the ions within the laser pulse duration. However, very little is known about the speed of electron localization out of an electron gas in correlated metals, i.e., the capture of an electron by an ion. Here, we demonstrate by means of pump-probe x-ray techniques across the Eu L_3 absorption edge that an electron localization process in the $\text{EuNi}_2(\text{Si}_{0.21}\text{Ge}_{0.79})_2$ intermetallic material occurs within a few hundred femtoseconds after the optical excitation. Spectroscopy and diffraction data collected simultaneously at low temperature and for various laser fluences show that the localization dynamics process is much faster than the thermal expansion of the unit cell along the c direction which occurs within picoseconds. Nevertheless, this latter process is still much slower than pure electronic effects, such as screening, and the subpicosecond timescale indicates an optical phonon driven origin. In addition, comparing the laser fluence dependence of the electronic response with that found in other intermediate $4f$ valence materials, we suggest that the electron localization process observed in this Eu-based correlated metal is mainly related to changes in the $4f$ hybridization. The observed ultrafast electron localization process sparks fundamental questions for our understanding of electron correlations and their coupling to the lattice.

DOI: [10.1103/PhysRevResearch.3.033211](https://doi.org/10.1103/PhysRevResearch.3.033211)

I. INTRODUCTION

Valence fluctuations in $4f$ electron systems have been studied intensively in the past, particularly focusing on heavy fermion behavior, Kondo insulators, magnetic order, the

occurrence of non-Bardeen-Cooper-Schrieffer-like superconductivity, and non-Fermi-liquid states [1]. However, valence transitions and their fluctuations are still not well understood, even for a prototypical system such as elemental cerium, which exhibits a first order valence transition as a function of pressure [2]. Many correlated metals are based on the fact that the f electron shell is partly occupied with $4f$ states lying at the Fermi surface. Therefore, hybridization with the conduction electrons plays a significant role in the structure, electronic, and magnetic properties, and it has been a field of condensed matter which reveals novel materials.

Here we draw our attention to the $\text{EuNi}_2(\text{Si}_{1-x}\text{Ge}_x)_2$ system, which exhibits an excellent playground to investigate valence transition [3], due to its dependences on temperature

*These authors contributed equally to this work.

†urs.staub@psi.ch

Published by the American Physical Society under the terms of the Creative Commons Attribution 4.0 International license. Further distribution of this work must maintain attribution to the author(s) and the published article's title, journal citation, and DOI.

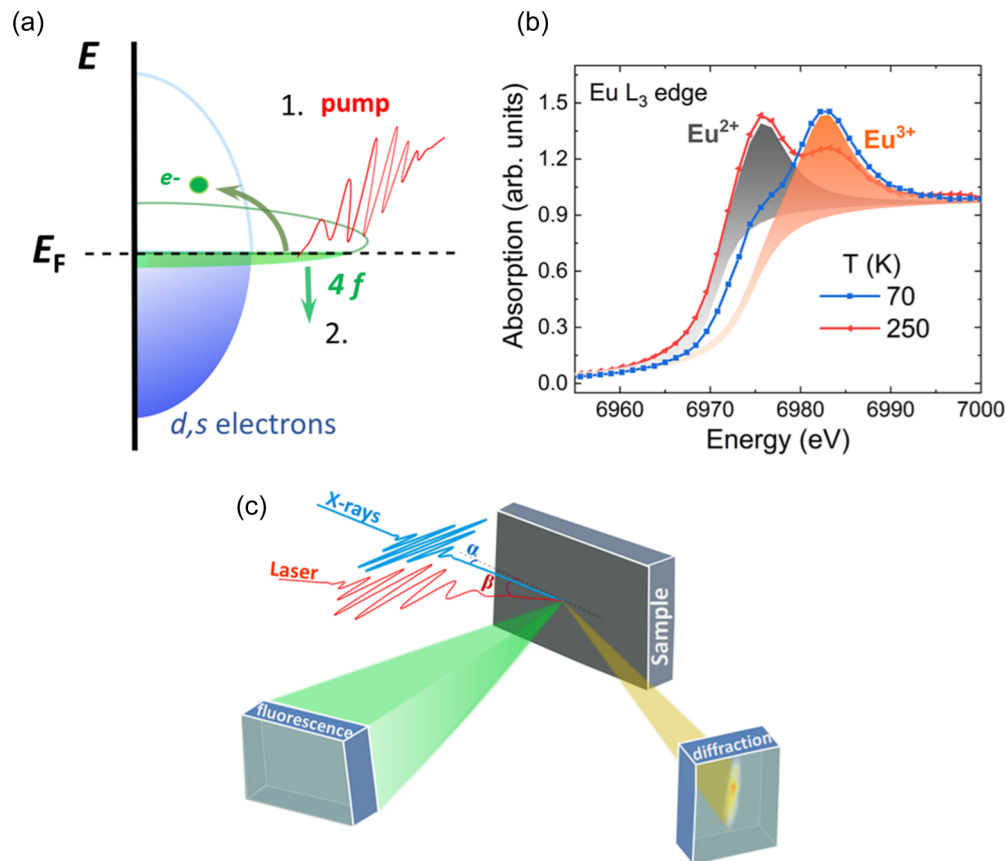


FIG. 1. Laser pump x-ray probe experiment. (a) Schematic of the conduction band and modifications of the 4f states upon laser excitation. (b) Eu L_3 edge XAS spectra below (blue) and above (red) the valence-transition temperature. The peaks located at 6.977 and 6.983 keV are assigned to the Eu $2p_{3/2} \rightarrow 5d$ dipole transition (L_3 edge) of Eu²⁺ and Eu³⁺ ions, respectively. (c) Sketch of the time-resolved x-ray diffraction/absorption experimental setup. The incident angles α and β for the x rays and laser are 0.5° and 5°, respectively.

[4,5]; magnetic field [6]; on the substitutional level x [7], which acts as internal pressure [3]; and on applied external pressure [8,9]. While the Eu valence is closer to 3+ for temperatures below the phase transition, it is closer to 2+ above the phase transition [4]. The transition is further associated with a large change in the crystal lattice volume. Electrons localized at the Eu ion reduce the attractive potential of the ion, which increases its ionic radius, resulting in a very strong electron-lattice coupling [4]. Analogous to increasing temperature, the amount of the Eu²⁺ ions (localized electrons) increases with increasing magnetic fields [4]. Despite Eu³⁺ having a nonmagnetic $J = 0$ ground state, the Eu ions have a spin $S = 3$ and angular momentum $L = -3$. Hence, magnetic excitation is observed throughout the valence transition in the EuCu₂(Si/Ge)₂ analog [10]. The decrease of the Eu valence with increasing temperature is an interesting aspect for a valence transition as it is opposite to the effect observed in correlated metals, such as YbAgCu₄ [11,12], YbInCu₄ [13], or SmB₆ [14], where the lanthanide valence increases with increasing temperatures. In the latter systems, these findings are interpreted as a strong reduction in hybridization between the f and d electrons at elevated temperatures.

Therefore, the EuNi₂(Si_{1-x}Ge_x)₂ system is an ideal case to probe how fast electrons can localize from the conduction band. X-ray absorption spectroscopy (XAS) at the Eu L_3

edge is a well-known and powerful tool to study the electron count at the Eu ion and has already been applied in detail in the static EuNi₂(Si_{1-x}Ge_x)₂ [3] and other Eu-based systems [6]. To study the dynamics, we selected the stoichiometry of $x = 0.79$, which results in a material with a valence-transition temperature (T_5) around 100 K; i.e., above and below T_5 the system is dominated by Eu²⁺ and Eu³⁺ ions, respectively. Exciting this material with an intense femtosecond (fs) laser pulse must result in a very intriguing charge localization, at least on long timescales after the electronic and lattice subsystems are equilibrated, and therefore the effective temperature is increased and the lattice volume is expanded. A simple schematic of the electronic states is shown in Fig. 1(a). The valence instability is caused by localized 4f states that lie at the Fermi surface E_F . An increase of 4f level occupation (decrease of the Eu valence) can therefore be obtained by the following mechanisms: (i) lowering the energy of the 4f states with respect to E_F or (ii) increasing the 4f electron bandwidth. Both processes can result in the transfer of conduction s - d electrons to localized f electrons. Recently, a light-induced valence transition has been confirmed by means of soft x-ray absorption spectroscopy at the Eu M_5 edge in which the Eu valence states were probed 50 ps after the photoexcitation [15]. However, the estimated timescale of the valence change was found to be much faster than 50 ps, which

was limited by the time resolution of the experiment, and no further information of how this fast valence change couples with the lattice could be obtained. Therefore, the origin and the timescale of the valence transitions and how they affect the crystal structure are remaining open problems that can be directly revealed by x-ray free electron laser experiments. In order to tackle such fast phenomena, we employ fs time-resolved (tr-) Eu L_3 -edge XAS.

II. EXPERIMENTS

Polycrystalline $\text{EuNi}_2(\text{Si}_{0.21}\text{Ge}_{0.79})_2$ samples have been grown by argon-arc melting and are described elsewhere [15]. The polycrystalline piece had dimensions of approximately $3 \times 4 \text{ mm}^2$ (and mass $\sim 49 \text{ mg}$). In order to obtain an optically shiny and flat surface, the sample was mechanically polished. Static spectroscopy XAS and magnetic susceptibility measurements to characterize the sample were performed at the SuperXAS-X10DA beam line at the Swiss Light Source and at the Laboratory for Multiscale Materials Experiments at PSI, respectively (see Appendix A).

Simultaneous time-resolved x-ray diffraction and XAS measurements were carried out at the Bernina instrument [16] of the SwissFEL facility using the optical pump/x-ray probe technique. A Si(111) double crystal monochromator was used to tune the x-ray energy around the Eu L_3 edge (6977 eV). The x-ray beam with a pulse duration of approximately 40–50 fs [full width at half maximum (FWHM)] was focused down to $30 \mu\text{m} \times 110 \mu\text{m}$ by using a pair of Kirkpatrick-Baez (KB) mirrors and the free electron laser (FEL) repetition rate was either 10 or 25 Hz.

The pump-probe experimental data were collected using three independent JUNGFRÄU (JF) pixel detectors [17] (a 1.5 megapixel (Mpixel) detector for the diffraction and an 0.5 Mpixel detector positioned at 90° of the incoming x-ray beam for absorption (fluorescence) measurements, and a third 0.5 Mpixel JUNGFRÄU served as an I0 intensity monitor (normalization) by collecting the scattering from Kapton foil placed into the incoming x-ray beam). A fourth detector was used to collect resonant inelastic x-ray scattering (RIXS) data, but these results/data are not included here. The JF detector for diffraction was positioned at approximately 280 mm from the sample position, just outside the chamber, allowing x rays to pass through a Kapton window. For each two-dimensional (2D) image recorded from one of the JF detectors, an individual common-mode offset correction was applied to reduce readout noise. This correction is different for every detector module and changes from shot to shot. In addition, a threshold was applied in order to remove all pixels with negative value. Further information regarding the JF detector can be found in Ref. [18] and references therein. For fluorescence, the whole JF detector area was integrated for each x-ray shot as there were no diffraction peaks visible on this detector. The integrated intensity was normalized by the I0 monitor.

The experiment was performed around a temperature of 90 K (below $T_S \sim 100 \text{ K}$). To reach this temperature, the sample was cooled with a helium cryojet that was placed inside a chamber with controlled helium atmosphere to avoid ice formation and to reduce x-ray scattering and absorption from the air. The temperature of the sample was monitored

during the experiment with a sensor that was calibrated using a Cernox temperature sensor positioned on the sample holder. Since the temperature sensor was not physically attached to the sample and the sample holder was made of a nonmetallic material to reduce heat losses, we believe the sample was cooled down around 90 K with an error bar of approximately $\pm 10 \text{ K}$.

The sample was excited by a 800 nm Ti:sapphire femtosecond laser with pulse duration of 45 fs FWHM, focal spot size of approximately $370 \times 230 \mu\text{m}^2$, and the fluence was varied between 2.5 and 12.5 mJ/cm^2 with the repetition rate half that of the x rays in order to alternately probe the pumped and unpumped sample. The fluence calibration of the pump laser was performed with a charge-coupled device camera mounted at the sample position in which the shape and beam size were monitored as a function of the laser power for different attenuations. The angle of incidence of the 800 nm pump laser was adjusted to 5° , in which previous reflectivity measurements (not shown here) indicated a penetration depth of approximately 30 nm. In order that the incoming x-ray beam interacts with the pumped sample volume, the sample was mounted at a grazing angle of approximately 0.5° , which reduced the x-ray penetration depth to also approximately 30 nm.

For each fluence and for selected photon energies, at least two time scans were collected from -5 to approximately 60 ps with 1000 shots per time delay. The data were filtered for very low and high intensity shots and then normalized by I0.

The optical pump-probe experiments were performed using a standard pump-probe configuration with an 800 nm Ti:sapphire laser beam split in two. Both laser beams arrive at the sample with p polarization in which the stronger one was responsible for photoexciting and the weaker one for probing the Eu-based material. The repetition rates of the probe and pump laser were 2 and 1 kHz, respectively, with a time resolution of approximately 120 fs (FWHM). The reflectivity change (ΔR) was recorded using a photodiode mounted close to the sample. The angle of incidence was approximately 17° . The $\text{EuNi}_2(\text{Si}_{0.21}\text{Ge}_{0.79})_2$ sample was mounted inside a low-vibration 4 K cryostat with quartz windows in which the sample was cooled down to 90 K, i.e., a few degrees below the valence transition and at similar temperatures compared to the pump and probe x-ray setup.

III. RESULTS AND DISCUSSION

Static XAS data taken above and below the valence transition are shown in Fig. 1(b), in which the results clearly exhibit the two Eu valence states. This method is extremely sensitive for quantifying the timescale of an electron localization process in the Eu $4f$ shell and allows us to provide a better understanding of the underlying mechanism on this $\text{EuNi}_2(\text{Si}_{0.21}\text{Ge}_{0.79})_2$ intermetallic compound. The XAS technique extracts the electronic information of the Eu ions, since the incoming x-ray radiation creates electric dipole transitions from the deep-core Eu $2p_{3/2}$ states to the unoccupied $5d$ bands in the presence of the core hole at the Eu L_3 edge. As the core electrons are excited to unoccupied low binding energy states in the presence of the core hole, these electrons are probing the density of d states close to the Fermi level that are projected

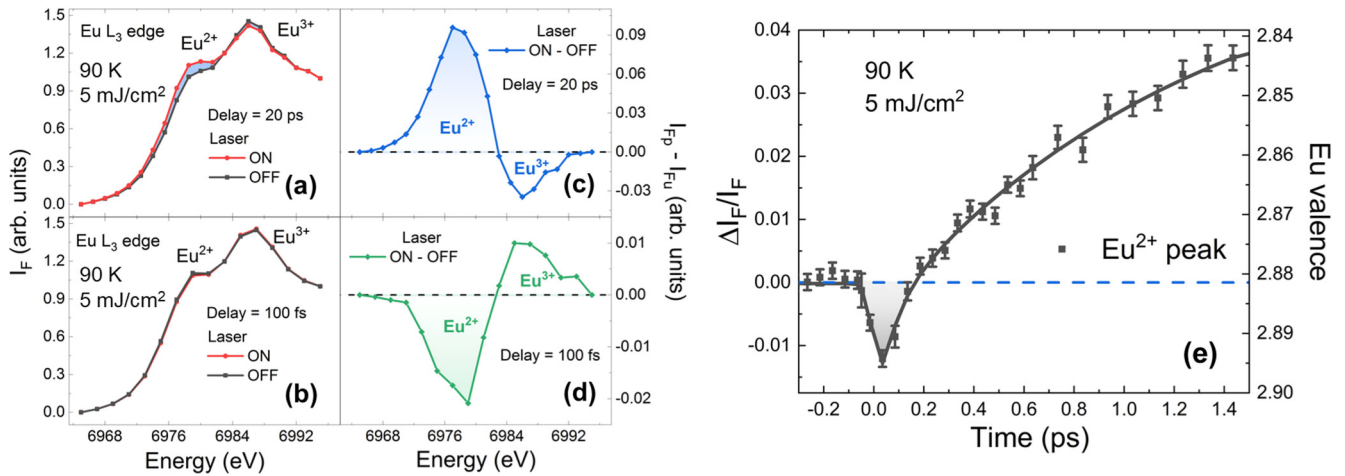


FIG. 2. Time-resolved x-ray absorption data with energies around the Eu L_3 edge taken at 90 K. Panels (a,b) exhibit the normalized XANES spectra for $\text{EuNi}_2(\text{Si}_{0.21}\text{Ge}_{0.79})_2$ from the excited (I_{Fp} , laser on) and unperturbed (I_{Fu} , laser off) sample for time delays of (a) 20 ps and (b) 100 fs. The laser fluence was adjusted to 5 mJ/cm^2 . Panels (c,d) show the difference between the unperturbed and transient absorption spectra at delays of 20 ps and 100 fs after excitation, respectively. Panel (e) displays the normalized intensity $[(I_{Fp} - I_{Fu})/I_F]$ collected at a fixed energy (at the Eu^{2+} resonance of 6.977 keV) as a function of time delay.

in space to the Eu site. The spatial extension is limited to the extension of the deep core hole wave functions ($2p$ hole) as the signal is proportional (given by the matrix element) to the overlap between the $2p$ and $5d$ states for the dipole transition. Due to the large Coulomb interaction between the $4f$ levels and the $5d$ states and the different screening of the d states for the different $4f$ level occupations, a 7 eV splitting occurs between the Eu valence states ($\text{Eu}^{2+}/\text{Eu}^{3+}$) in the XAS, as demonstrated in Fig. 1(b). There is more general information regarding the principle of XAS measurements in Ref. [19]. Note that the dynamics of the absorption process is limited by the lifetime of the $2p$ deep core hole, which is reflected by the width of the resonance (4 eV) which is, with approximately 1 fs, much faster than the studied dynamics and the valence fluctuations between the two Eu $4f$ valence occupations of the Eu^{2+} and Eu^{3+} states [3]. Therefore, quantitative information regarding Eu valence can be extracted from the XAS measurements, down to the low-fs time regime. In our studies the Eu valence states obtained from the dynamic measurements were extracted from a comparison to the static XAS data and evaluated as a function of time delay and fluence.

The tr-XAS experiment setup is sketched in Fig. 1(c). The Eu L_3 tr-x-ray absorption near-edge structure (tr-XANES) spectra of $\text{EuNi}_2(\text{Si}_{0.21}\text{Ge}_{0.79})_2$ are shown in Figs. 2(a) and 2(b) for a 20 ps and 100 fs time delay between the optical excitation and the x-ray probe, respectively. A clear change of the Eu^{2+} and Eu^{3+} resonances becomes apparent when plotting the differences between the transient and the unperturbed spectra, with opposite sign for the two delay times [Figs. 2(c) and 2(d)]. A time-delay scan performed up to 1.5 ps at the energy corresponding to the maximum of the Eu^{2+} resonance is shown in Fig. 2(e). It clearly illustrates that the x-ray fluorescence from the Eu^{2+} ions decreases promptly after the photoexcitation, consistent with an initial enhancement of the Eu valence (i.e., getting closer to $3+$). This obviously indicates that during the excitation process, localized $4f$ elec-

trons are removed from the f band and transferred to the itinerant conduction bands. In order to further investigate the time evolution of the valence states for different laser fluences, the system was photoexcited with different pump intensities. The results for selected fluences and timescales are shown in Fig. 3.

As displayed in Figs. 2 and 3, shortly after this initial suppression of the Eu^{2+} signal has recovered (at 200 fs for low fluences), the fluorescence signal from the Eu^{2+} ions surprisingly continues to increase with the same trend. This demonstrates an ultrafast-enhanced electron localization into the $4f$ states of the Eu ions beyond their initial state in a correlated electron system. Changes of the x-ray fluorescence at a given energy could also be due to ultrafast changes of the local atomic structure around the Eu ion represented by changes of, for example, the $5d$ final state crystal field splitting. However, the inversion on the amount of $\text{Eu}^{2+}/\text{Eu}^{3+}$ signal observed for different time delays [Figs. 2(c) and 2(d)] clearly indicates that the main changes are due to the Eu valence states rather than modification on the crystalline environment. In addition to this surprising enhancement of the Eu^{2+} component above its initial value, a clear change in the relaxation time is observed for different laser fluences, with higher fluences exhibiting a slower relaxation time (see direct comparison of two fluences in Fig. 4).

The observed ultrafast charge localization raises questions about the nature of the intrinsic process causing it. In a first step, the various modifications in the band structure consistent with the observed results can be evaluated as follows: (i) The $4f$ band energy could be lowered, (ii) the $4f$ bandwidth could be increased, or (iii) the hybridization between the $4f$ band and the conduction electrons could be affected. As the $4f$ states are well localized and not expected to be dispersive (momentum dependent), an increase of bandwidth would be directly related to an increase of hybridization. All the aforementioned scenarios directly result in a direct change of the

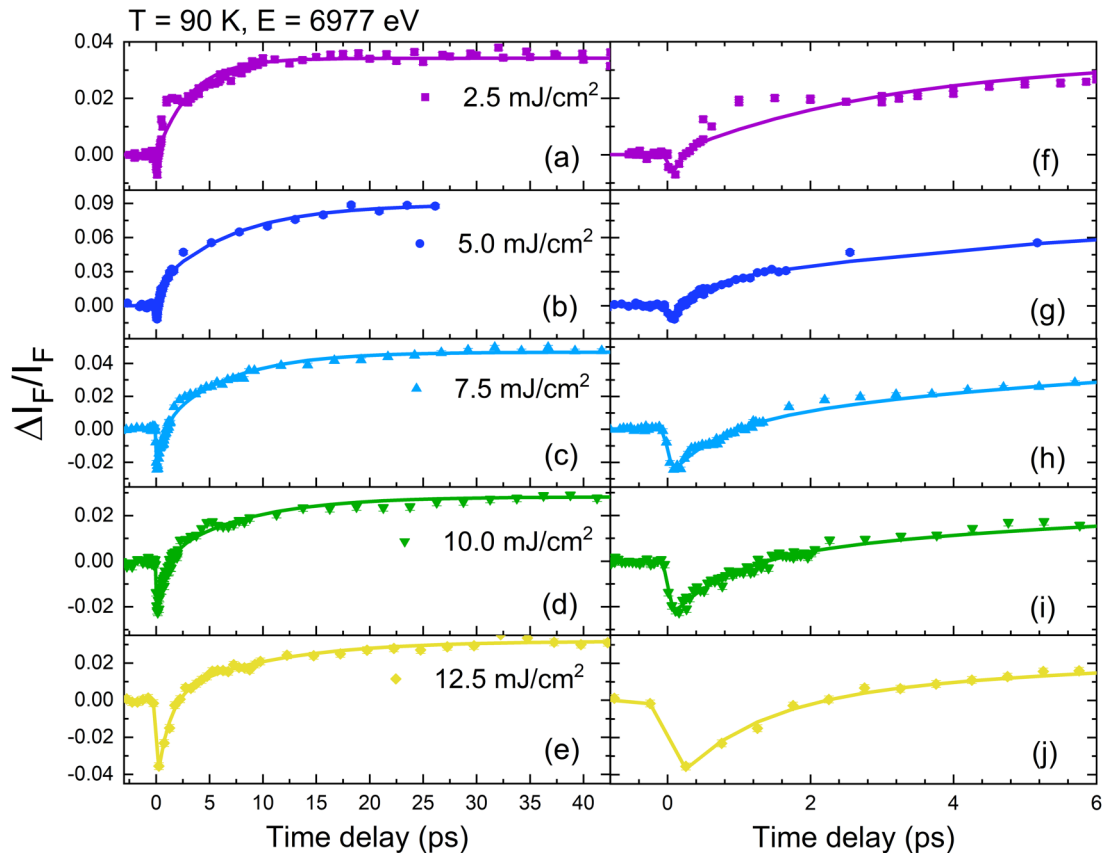


FIG. 3. Ultrafast fluorescence change ($\Delta I_F/I_F$) as a function of time delays for selected fluences at 90 K and x-ray energy beam tuned around the Eu^{2+} L_3 edge. Panels (a–e) show up to 42 ps and a short time behavior is shown in (f–j). The symbols and the solid lines are experimental data and fits as explained in the text, respectively.

$4f$ state's occupancy being the fundamental ingredient for electron localization. To gain more insight into this ultrafast valence change, we collected optical pump-probe reflectivity data at 90 K for various fluences with 800 nm pump and probe radiation (shown in Fig. 5). The optical reflectivity

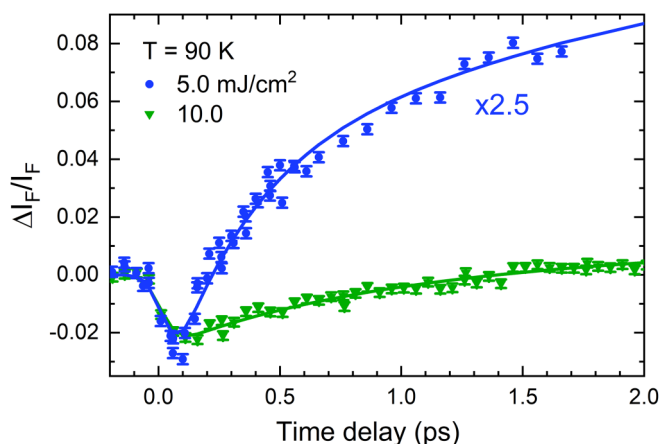


FIG. 4. Comparison between the fluorescence changes obtained at 90 K for laser fluences of 5 and 10 mJ/cm^2 up to 2 ps. The low-fluence data were multiplied by a factor of 2.5 to clearly indicate the timescales of the localization processes.

data show an intriguing sign change similar to that observed in the tr-XANES at a comparable fluence. The tr-XANES response (see Fig. 3) shows a slowing down of the charge localization process when the laser fluence is increased. A similar behavior, with higher signal to noise ratio (SNR), is also observed in the optical data [Fig. 5(a)]. This allows us to use the optical data for a more precise determination of the timescales and fluence dependence, without the need to have a microscopic model for the optical conductivity probed with 800 nm radiation. Using a phenomenological model based on exponential functions as explained in Appendix B, we extract the relaxation times (τ_1) of the signal with a positive amplitude (A_1) from both the optical and the x-ray data. The resulting time constants are plotted as a function of the excitation fluence in Fig. 5(b).

The relaxation time τ_1 increases approximately linearly as a function of fluence, which is in strong contrast to what has been reported in intermediate valent systems with strong $4f$ conduction band hybridization, such as YbAgCu_4 or SmB_6 [20,21], where the relaxation time strongly decreases for increasing fluence. This decrease for the latter systems has been interpreted in terms of a reduction of the $4f$ conduction band hybridization. In other words, the relaxation time of these correlated metals approaches much faster response times of an uncorrelated metal when either the temperature or the pump fluence is increased [20,21].

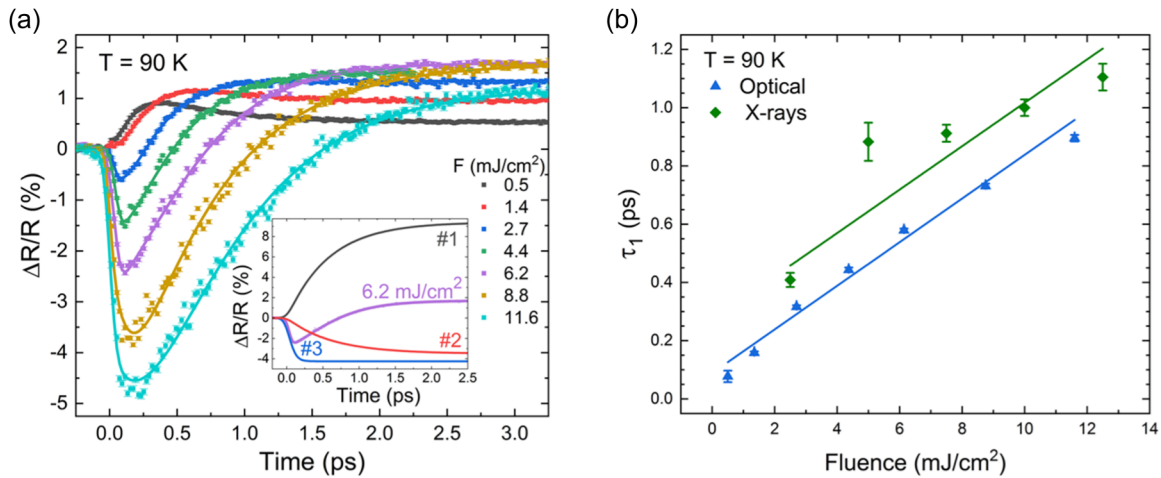


FIG. 5. Optical pump-probe measurements. Panel (a) shows the transient 800 nm reflectivity as a function of fluence collected at 90 K. The inset shows the three exponential curves employed to fit the data. Panel (b) shows the fluence dependence of the recovery time τ_1 obtained from the x-ray and optical measurements at 90 K. The solid green and blue lines represent linear fits.

However, the $\text{EuNi}_2(\text{Si}_{0.21}\text{Ge}_{0.79})_2$ system presents contrasting behavior compared to YbAgCu_4 or SmB_6 , which leads us to suggest that in the Eu-based material system an external stimulus, i.e., the photoexcitation, increases the $4f-d$ (s) hybridization. This contrast behavior in the photoexcitation response between these classes of materials is likely connected to the opposite temperature dependence of the lanthanide valence between these materials. While the valence increases, for instance, in YbAgCu_4 with increasing temperature [$\text{Yb}^{2+}(4f^{14}) \rightarrow \text{Yb}^{3+}(4f^{13})$] [22], it decreases in the case of $\text{EuNi}_2(\text{Si}_{0.21}\text{Ge}_{0.79})_2$. In addition, we point out that such systems are known to display heavy fermion and Kondo behavior, which is absent in the case for the Eu-based material investigated here [23,24]. Despite such contrasting behavior on the evolution of the timescales, Kondo, heavy fermion behavior, and valence fluctuations are phenomena with similar origin, i.e., defined by strong interactions between the localized f and the itinerant conduction electrons.

Even if the changes of the electronic structure are caused by an increase of the hybridization in the system, it remains to explain why the electronic structure is also modified. Assuming a purely electronic effect (such as screening) to be at its origin, a much faster change of electron localization would be expected [25]. This is not consistent with the observed instantaneous process of electron delocalization during the laser excitation for pump fluences used in the x-ray experiment. Note that the optical data give us some hints towards a threshold behavior, as fluences less or equal to 1.4 mJ/cm^2 do not show an instant drop of the reflectivity data (Fig. 5). Independent of this signature, it is important to consider the induced lattice dynamics, in particular as the electron localization is strongly coupled to it. We expect three major processes that could be important to consider: (1) lattice expansion, (2) coherent excitation of a specific phonon mode, or (3) coupling to random lattice fluctuations represented by Debye-Waller terms measurable in x-ray diffraction. In order to investigate how the electrons and the lattice are entangled, and to shine light on the aforementioned processes, we recorded simulta-

neously to the fluorescence XAS signal x-ray diffraction data of the (002) Bragg reflection.

The 2D diffraction images of the (002) peak were collected for each x-ray pulse, accumulating the same number of laser-on (perturbed) and laser-off (unperturbed) images per time delay as exhibited in Fig. 6. The images were first filtered for low-intensity x-ray pulses and then averaged for each time delay. At a given x-ray energy and pump fluence, at least two time-delay scans with approximately 1000 shots per step were collected. To extract a one-dimensional (1D) profile as a function of total scattering angle 2θ (as shown in Figs. 7 and 9), each averaged 2D image was integrated along the azimuthal angle. Figure 6(c) shows the displacement of the (002) Bragg peak photoexcited with a pump of 7.5 mJ/cm^2 for two different time delays. The difference between perturbed and unperturbed normalized intensity is shown in Fig. 6(d).

Figure 7(a) shows the (002) intensity projected to the 2θ axis for various time delays with a pump fluence of 7.5 mJ/cm^2 . Clear changes in the peak position are observed Fig. 7(b), which can be directly transferred to changes of the unit cell volume [Fig. 7(c)] under the assumption that only the out of surface direction is affected by the excitation. In addition, Fig. 8 shows a detailed time evolution of the intensity and width for the (002) Bragg reflection for a fluence of 7.5 mJ/cm^2 obtained from the fit to a Gaussian function in which the lattice response is delayed compared to the changes in the valence. Similar behavior is also observed for a lower fluence of 2.5 mJ/cm^2 (see Fig. 9). A strong increase in width is observed when the system is perturbed [Fig. 8(a)]; however, the ratio between the integrated intensity for laser-on and -off only shows a monotonic behavior [Fig. 8(b)] as a function of time delay and has insufficient precision to observe a possible ultrafast small interatomic motion at short time delays. The width changes are directly correlated to the peak motion that shows a maximum around 25 ps. Since the probing depth of the x rays and the penetration depth of the optical excitation are approximately equal, the x rays probe a distribution of excitation fluences, which consequently broadens the peak profile as observed in Fig. 8(a).

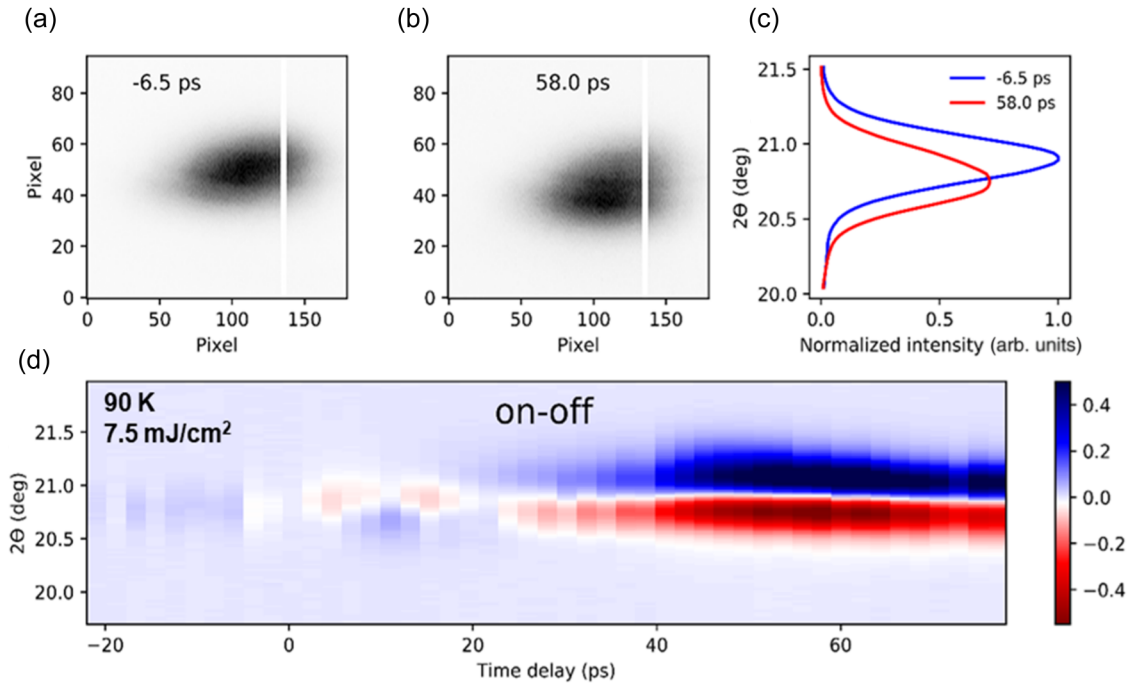


FIG. 6. (002) Bragg reflection measured at 90 K. (a) Before time zero at -6.5 ps and (b) at 58 ps after laser excitation with a fluence of 7.5 mJ/cm^2 . Panel (c) displays the normalized (002) peak profile resulting from the azimuthal integration. Panel (d) is a normalized temporal evolution of the difference between the perturbed (laser-on) and unperturbed (laser-off) peak intensity obtained with a laser fluence of 7.5 mJ/cm^2 .

To extract the lattice volume change, we assume that at early timescales, the in-plane directions remain locked to the underlying undisturbed bulk lattice. The diffraction data also show that the lattice dynamics has similar reversal behaviors as the valence dynamics observed by the XAS technique: an initial small and relative fast compression (around a few ps) followed by an expansion of the lattice at latter times (dozens of ps). The initial charge delocalization at the Eu ions, which is faster than 100 fs, triggers the lattice to contract because the ionic radius of the Eu ions collapses (Eu^{2+} ionic radius is larger than for Eu^{3+}). After a few hundred fs of the photoexcitation, the Eu valence has already decreased above the initial

value, and correspondingly the Eu ionic radius is larger than its undisturbed value leading to opposite forces on the lattice. As the lattice volume change is represented by an acoustic mode, the forces on the atoms first slow down the already moving atoms, and after they come to rest, accelerate them in the opposite direction. This scenario can be represented by a simple damped harmonic oscillator. The peak in the unit cell volume expansion around 30 ps represents an overshoot of the lattice expansion (damped acoustic mode) as the valence transition has been mainly completed at that time and the valence (or $\Delta I_F/I_F$ signal) reached almost saturated values [Figs. 7(b) and 7(c)]. However, it also shows a weak maximum

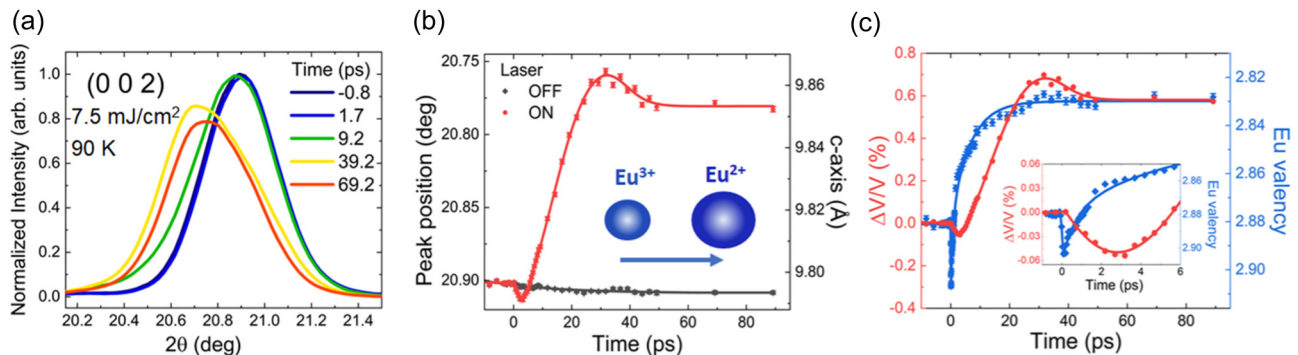


FIG. 7. Time-resolved x-ray diffraction. (a) (002) Bragg reflection intensities at various time delays after photoexcitation with a fluence of 7.5 mJ/cm^2 taken at 90 K. (b) Fitted (002) peak position and corresponding crystallographic c -axis lattice constant as a function of time for perturbed (red symbols) and unperturbed system (gray symbols). The inset shows schematically the increase of the ionic radii between Eu^{2+} ions and Eu^{3+} after excitation. (c) Relative expansion of the chemical unit cell along the c axis and the Eu valency as a function of time. Inset: Zoom into short delay times of (c).

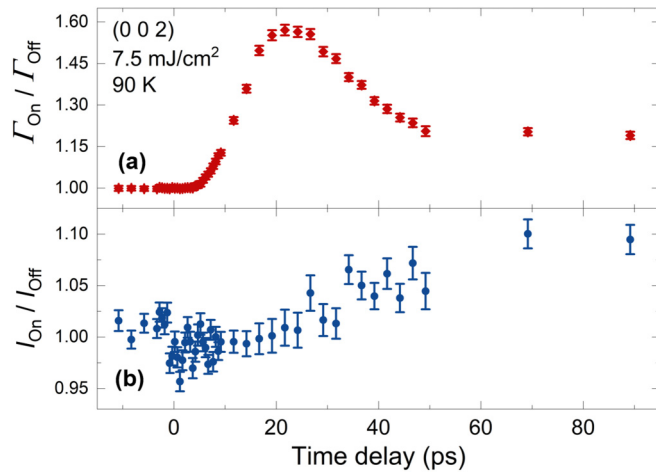


FIG. 8. (002) Bragg peak analysis at 90 K and fluence of 7.5 mJ/cm^2 . Temporal relative change of the ratio between the (a) Γ (FWHM) with laser on and off and the (b) integrated intensity I with laser on and off ($I_{\text{on}}/I_{\text{off}}$).

at these times. This shows that at the tens of ps timescales the crystal structure is dragging the electronic structure as is the case for the static, pressure-induced valence change. In general, these results clearly show that the lattice volume dynamics is much slower and delayed compared to the change in valence. This decoupling strongly proves that the electron localization drives the lattice motion and not vice versa, except, as mentioned before, at the times where it overshoots it might drag a small valence change with it [see Figs. 7(b) and 7(c)].

The second scenario, i.e., the coherent excitation of a specific phonon mode could also be tested by x-ray diffraction, as it would result in oscillatory intensity changes of the Bragg peaks as a function of time. Nevertheless, no such effects on the (002) reflection intensity within the experimental accuracy are observed below 1 ps (Fig. 8). Note that the expected changes on a low Q reflection are much smaller than the errors of the observed intensities preventing us from drawing any clear conclusions from the diffraction intensity data. However,

the excitation of a coherent phonon mode with a frequency below 6 THz (frequency limited by the time resolution of the optical experiment) would most likely be visible in the optical data. While the optical data show changes with a similar timescale as observed in the XAS measurements, no coherent modulations are visible. In addition, considering the quartic response on the mode amplitude, as observed, e.g., by ultrafast x-ray diffraction in cuprates [26] or pnictides [18], a fast initial change on the order of a quarter period of the mode frequency would be expected, which is inconsistent with our data.

The third scenario, i.e., the coupling to random lattice fluctuations would lead to a clear decay of diffraction intensity due to the Debye-Waller term. Unfortunately, our x-ray data are inconclusive, as this effect is expected to be very small for low Q reflections, such as the (002) reflection. However, the observed timescale is on the order of the timescale expected for the energy transfer between the electronic subsystem to the lattice, which suggests that lattice fluctuations are likely involved in the electron localization process.

An incoherent interaction between the lattice and the electron localization brings up interesting considerations. First, there is a large angular magnetic moment change between the two Eu valence states (see Fig. 10 in Appendix A). Since angular momentum is conserved, the electron localization process must transfer the momentum from/to the lattice. Ultrafast angular momentum transfer from the magnetization of a ferromagnetic Fe film to the lattice has recently been detected through ultrafast x-ray diffraction that observed the creation of an acoustic shear wave [27]. The transition from a Eu^{3+} ($J = 0$, $L = -3$, and $S = 3$) to a Eu^{2+} state ($J = 7/2$, $L = 0$, and $S = 7/2$), requires the total annihilation of a large angular magnetic moment at the Eu sites, which are randomly oriented due to the absence of magnetic long-range order. A moment transfer to/from the lattice would result in an incoherent creation/annihilation of phonons. Therefore, it is possible that an angular magnetic moment transfer acts as a bottleneck for the electron localization in such metallic systems. However, the initial state is in a valence fluctuating regime and the fastest timescale observed at the lowest fluence might be related to the timescale of the ground state valence fluctuations.

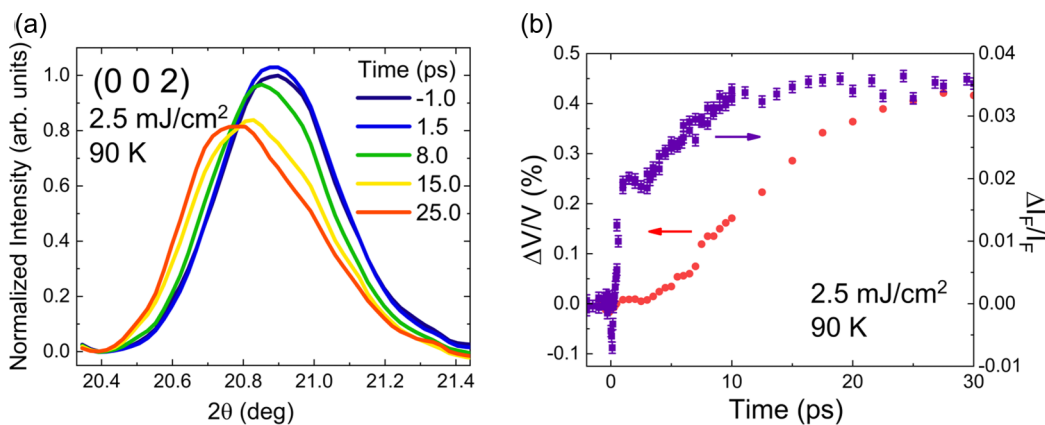


FIG. 9. Time-resolved x-ray diffraction and absorption measurements at 90 K and with a photoexcitation of 2.5 mJ/cm^2 . (a) (002) Bragg reflection intensities at selected time delays. (b) Relative expansion of the chemical unit cell along the c axis ($\Delta V/V$) and the ultrafast fluorescence change ($\Delta I_F/I_F$) as a function of time delays up to 30 ps.

IV. CONCLUSIONS

We presented a series of pump-probe optical reflectivity, fs time-resolved x-ray absorption spectroscopy measurements at the Eu L_3 edge, and x-ray diffraction collected on the (002) Bragg peak for the valence transition $\text{EuNi}_2(\text{Si}_{0.21}\text{Ge}_{0.79})_2$ intermetallic compound. Our findings show that after a first prompt initial valence increase of the Eu ions towards the 3+ oxidation state, the valence monotonically decreases towards the Eu^{2+} ions with unexpected subpicosecond timescales. This can be directly related to a fast charge delocalization followed by a charge localization with subpicosecond timescales which is shown to be significantly fluence dependent. This ultrafast electron localization of electrons out of the conduction band is consistent with an increase of $s-d-f$ hybridization at the Fermi level. The diffraction investigation shows a remarkably delayed response of the volume expansion that is driven by a charge localization process. These findings raise a series of fundamental questions for correlated electron systems and their dynamics.

Experimental and model data are accessible from the Materials Cloud Archive [28].

ACKNOWLEDGMENTS

We would like to acknowledge Kojiro Mimura, Matteo Savoini, Valerio Scagnoli, and Maarten Nachtegaal for informative discussions. Time-resolved x-ray measurements were carried out at the Bernina end station of the SwissFEL facility, Paul Scherrer Institute (PSI), Switzerland. X-ray absorption characterization experiments were performed at the SuperXAS beamline of the Swiss Light Source (SLS), PSI. Optical pump-probe data were measured at the FEMTO-microXAS laser system at SLS, PSI. This work was supported by NCCR Molecular Ultrafast Science and Technology (NCCR MUST No. 51NF40-183615) and NCCR MARVEL, research instruments of the Swiss National Science Foundation (SNSF) and the SNF Project No. 200021_169017. This work was supported by MEXT Quantum Leap Flagship Program (MEXT Q-LEAP) Grant No. JPMXS0118068681 and by JSPS KAKENHI Grant No. 19H05824. We also acknowledge support of the European Research Council Advanced Grant No. H2020 ERCEA 695197 DYNAMOX.

APPENDIX A

Static x-ray absorption near-edge structure (XANES) measurements were performed around the Eu L_3 absorption edge as a function of temperature above and below the valence phase transition (T_s). These measurements were carried out

at the SuperXAS-X10DA beamline at SLS (PSI, Switzerland). The polychromatic beam from the 2.7 T bending magnet was collimated using a Si-coated collimating mirror at 2.5 mrad (which also served to suppress higher harmonics), monochromatized by a Si(111) channel-cut monochromator, and subsequently focused by a Rh-coated toroidal mirror to a spot size of $100 \times 100 \mu\text{m}$ on the sample position. The sample was cooled down using a He cryostream mounted on a nonmetallic sample holder placed inside a chamber with Kapton window and purged with N_2 . The sample temperature was monitored using a Cernox sensor positioned on the sample holder and previously characterized. Since the sample temperature could not be monitored in real time, we estimated an error bar of approximately ± 10 K. The fluorescence signals were recorded using a five-element silicon drift detector (SDD) installed at 90° to the incident beam and positioned around 300 mm from the sample. A Cr filter was added in front of the detector to additionally reduce the background and to reduce the fluorescence intensity to keep the detector in a linear regime. As shown in Fig. 10(a), the Eu L_3 XAS spectrum shows two peaks separated by approximately 7 eV due to the two possible Eu valence states. In order to obtain information about the average valence, the amount of $\text{Eu}^{2+}/\text{Eu}^{3+}$ was determined by fitting the absorption spectra using the DEMETER software as displayed in Fig. 10(b) [4]. The evolution of the Eu valence state for selected temperatures is summarized in Fig. 10(c) in which a clear phase transition is observed around 100 K.

Magnetization measurements were also performed using a commercial superconducting quantum interference device (SQUID) magnetometer at the Laboratory for Multiscale Materials Experiments at PSI. The macroscopic measurements were performed in a temperature range from 50 to 300 K in which a constant magnetic field of 0.1 T was applied. Our macroscopic measurements shown in Fig. 10(d) agree quite well with the data reported in Ref. [5]. From these aforementioned static measurements, the valence-transition temperature was confirmed around $T_s \sim 100$ K for the $\text{EuNi}_2(\text{Si}_{0.21}\text{Ge}_{0.79})_2$ sample.

APPENDIX B

The time-resolved reflectivity change was fitted with three exponential functions (Fig. 11) for all traces convoluted with the instrument response function. The main goal of this purely phenomenological description is to extract a more precise timescale of the components that are very similar to the ones observed with the XAS data. The response function is described by the following equation:

$$S = \text{IRF}(t) \otimes \left[\left(A_1 \left\{ 1 - \exp \left[-\frac{(t-t_0)}{\tau_1} \right] \right\} + A_2 \left\{ 1 - \exp \left[-\frac{(t-t_0)}{\tau_2} \right] \right\} + A_3 \left\{ 1 - \exp \left[-\frac{(t-t_0)}{\tau_3} \right] \right\} \right) H(t) \right]$$

where \otimes is the convolution operator, $\text{IRF}(t)$ is the instrument response function assumed to be Gaussian, and $H(t)$ is the Heaviside function. The amplitudes and the relaxation time constants are expressed as A_i and τ_i , respectively. The

amplitude A_2 and the relaxation time τ_2 were kept constant at -0.57 and 0.82 ps, respectively, and these values were extracted from the fit obtained with the lowest fluence ($0.5 \text{ mJ}/\text{cm}^2$).

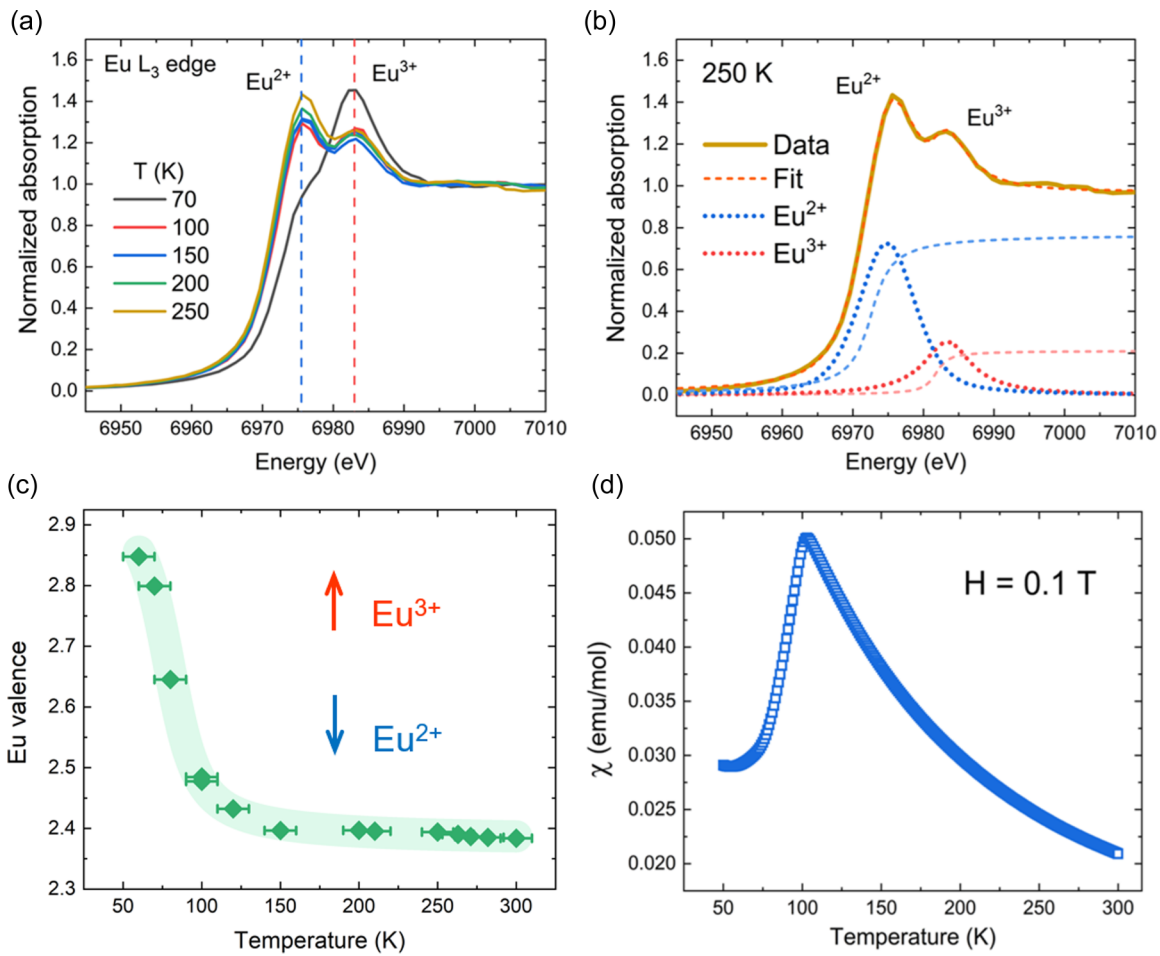


FIG. 10. Static sample characterization. Panels (a,b) show the x-ray absorption near-edge structure (XANES) data. Panel (a) displays selected XANES spectra for various temperatures. Panel (b) XANES data collected at 250 K with fits to the experimental data (dashed lines) to extract the Eu average valence. Thick dotted lines represent the white lines, and thin lines the atomic step functions. Panel (c) displays the temperature dependence of the Eu valence. Solid green line is a guide for the eye and a confidentiality range. (d) The magnetic susceptibility as a function of temperature carried out under a magnetic field of 0.1 T.

In analogy with the XAS data, we find that the physical origin of the first component $[F(A_1, \tau_1)]$ represents the valence increase as it has the same temporal behavior as the XAS component [Figs. 5(b) and 10(b)]; i.e., it increases as a func-

tion of time. The second component $[F(A_2, \tau_2)]$ is unclear, as we do not have comparable XAS data at very low fluence, where this component is well defined. Finally, the third component $[F(A_3, \tau_3)]$ represents the fast initial component, and is

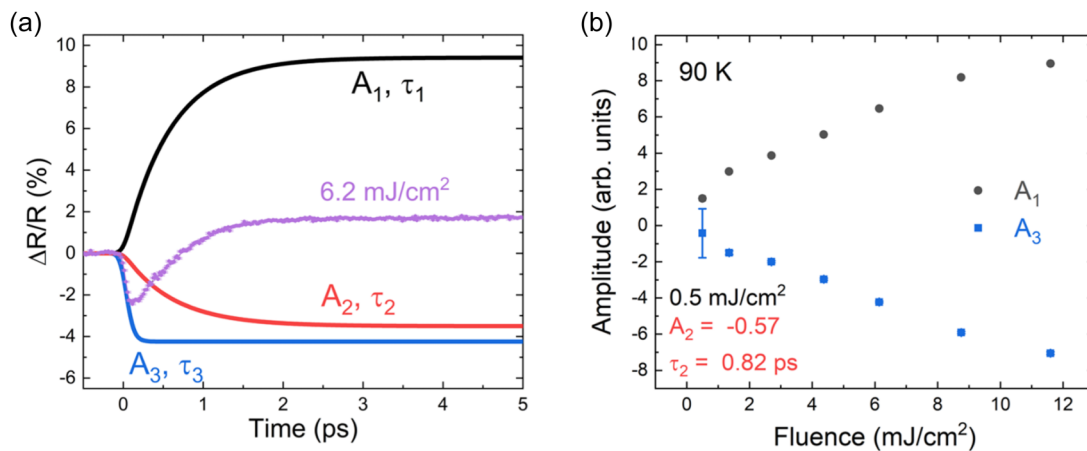


FIG. 11. 90 K optical reflectivity data. (a) The three exponential curves employed to fit the optical data at 6.2 mJ/cm². (b) Evolution of the A₁ and A₂ amplitudes as a function of fluence. Blue inset in (b) shows the fixed amplitude (A₃) and relaxation time (τ₃) used to fit the data.

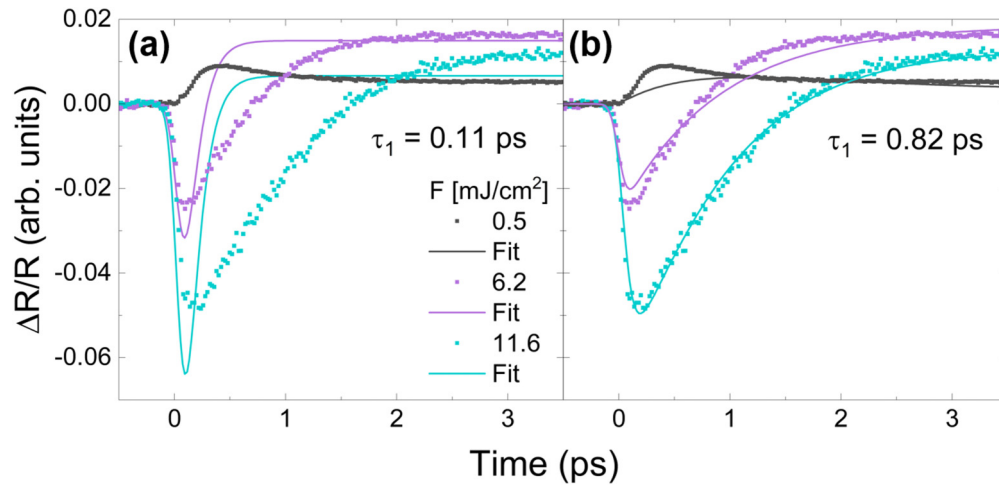


FIG. 12. Optical pump-probe data for selected fluences at 90 K. Panels (a,b) show the experimental and attempted fits performed with the τ_1 component fixed at 0.11 and 0.82 ps, respectively. The fits were performed with the attributes A_2 and τ_2 set free.

associated with an initial charge delocalization process that is also visible in the XAS data.

Panel (a) in Fig. 11 shows the experimental data collected at 6.2 mJ/cm² and the three exponential functions used to fit the reflectivity data. The extracted amplitudes A_1 and A_3 as a function of fluence taken at 90 K are shown in panel (b) of Fig. 11. The amplitudes A_1 (A_3) increase (decrease) linearly as a function of fluence.

As previously mentioned, the relaxation time τ_2 was kept constant while τ_1 was released in order to fit our experimental

data. To rule out that the increase in τ_1 is not an artifact from keeping the second component fixed, a fit was performed keeping the components A_2 and τ_2 free and τ_1 fixed. Figure 12 displays the fits assuming the relaxation time τ_1 fixed as the one obtained at low fluence of 0.11 ps [Fig. 12(a)] and high fluence of 0.82 ps [Fig. 12(b)]. As observed in Figs. 12(a) and 12(b), the fits for different fluences show poor agreement with the experimental data for different fluences. Therefore, at the relaxation time τ_1 has to increase as a function of fluence.

- [1] J. M. Lawrence, P. S. Riseborough, and R. D. Parks, Valence fluctuation phenomena, *Rep. Prog. Phys.* **44**, 1 (1981).
- [2] D. C. Koskenmaki and K. A. Gschneidner, Cerium, in *Handbook on the Physics and Chemistry of Rare Earths*, Vol. 1, edited by K. A. Gschneidner Jr. and L. Eyring (Elsevier, Amsterdam, 1978), p. 337.
- [3] G. Wortmann, I. Nowik, B. Perscheid, G. Kaindl, and I. Felner, Critical evaluation of Eu valences from L_{III}-edge x-ray-absorption and Mössbauer spectroscopy of EuNi₂Si_{2-x}Ge_x, *Phys. Rev. B* **43**, 5261 (1991).
- [4] H. Wada, T. Sakata, A. Nakamura, A. Mitsuda, M. Shiga, Y. Ikeda, and Y. Bando, Thermal expansion and electrical resistivity of EuNi₂(Si_{1-x}Ge_x)₂, *J. Phys. Soc. Jpn.* **68**, 950 (1999).
- [5] K. Ichiki, K. Mimura, H. Anzai, T. Uozumi, H. Sato, Y. Utsumi, S. Ueda, A. Mitsuda, H. Wada, Y. Taguchi, K. Shimada, H. Namatame, and M. Taniguchi, Hard x-ray photoemission study of the temperature-induced valence transition system EuNi₂(Si_{1-x}Ge_x)₂, *Phys. Rev. B* **96**, 045106 (2017).
- [6] Y. H. Matsuda, Z. W. Ouyang, H. Nojiri, T. Inami, K. Ohwada, M. Suzuki, N. Kawamura, A. Mitsuda, and H. Wada, X-Ray Magnetic Circular Dichroism of a Valence Fluctuating State in Eu at High Magnetic Fields, *Phys. Rev. Lett.* **103**, 046402 (2009).
- [7] K. S. Nemkovski, D. P. Kozlenko, P. A. Alekseev, J. M. Mignot, A. P. Menushenkov, A. A. Yaroslavtsev, E. S. Clementyev, A. S. Ivanov, S. Rols, B. Klobes, R. P. Hermann, and A. V. Griбанov, Europium mixed-valence, long-range magnetic order, and dynamic magnetic response in EuCu₂(Si_xGe_{1-x})₂, *Phys. Rev. B* **94**, 195101 (2016).
- [8] H. J. Hesse, R. Lubbers, M. Winzenick, H. W. Neuling, and G. Wortmann, Pressure and temperature dependence of the Eu valence in EuNi₂Ge₂ and related systems studied by Mössbauer effect, X-ray absorption and X-ray diffraction, *J. Alloys Compd.* **246**, 220 (1997).
- [9] H. Wada, M. F. Hundley, R. Movshovich, and J. D. Thompson, Pressure effect on the valence transition of EuNi₂(Ge_{1-x}Si_x)₂, *Phys. Rev. B* **59**, 1141 (1999).
- [10] P. A. Alekseev, K. S. Nemkovski, J. M. Mignot, V. N. Lazukov, A. A. Nikonov, A. P. Menushenkov, A. A. Yaroslavtsev, R. I. Bewley, J. R. Stewart, and A. V. Griбанov, Magnetic excitations in EuCu₂(Si_xGe_{1-x})₂: From mixed valence towards magnetism, *J. Phys.: Condens. Matter* **24**, 375601 (2012).
- [11] J. M. Lawrence, G. H. Kwei, P. C. Canfield, J. G. DeWitt, and A. C. Lawson, L_{III} x-ray-absorption in Yb compounds: Temperature dependence of the valence, *Phys. Rev. B* **49**, 1627 (1994).
- [12] C. Dallera, M. Grioni, A. Shukla, G. Vanko, J. L. Sarrao, J. P. Rueff, and D. L. Cox, New spectroscopy solves an old puzzle: The Kondo scale in heavy fermions, *Phys. Rev. Lett.* **88**, 196403 (2002).
- [13] C. Dallera, M. Grioni, A. Shukla, G. Vanko, and J. L. Sarrao, Truly bulk-sensitive spectroscopic measurements of valence in heavy fermion materials, *J. Synchrotron Radiat.* **9**, 242 (2002).

- [14] M. Mizumaki, S. Tsutsui, and F. Iga, Temperature dependence of Sm valence in SmB_6 studied by X-ray absorption spectroscopy, *J. Phys. Conf. Ser.* **176**, 012034 (2009).
- [15] Y. Yokoyama, K. Kawakami, Y. Hirata, K. Takubo, K. Yamamoto, K. Abe, A. Mitsuda, H. Wada, T. Uozumi, S. Yamamoto, I. Matsuda, S. Kimura, K. Mimura, and H. Wadati, Photoinduced valence dynamics in $\text{EuNi}_2(\text{Si}_{0.21}\text{Ge}_{0.79})_2$ studied via time-resolved x-ray absorption spectroscopy, *Phys. Rev. B* **100**, 115123 (2019).
- [16] G. Ingold, R. Abela, C. Arrell, P. Beaud, P. Bohler, M. Cammarata, Y. P. Deng, C. Erny, V. Esposito, U. Flechsig *et al.*, Experimental station Bernina at SwissFEL: Condensed matter physics on femtosecond time scales investigated by X-ray diffraction and spectroscopic methods, *J. Synchrotron Radiat.* **26**, 874 (2019).
- [17] F. Leonarski, A. Mozzanica, M. Brückner, C. Lopez-Cuenca, S. Redford, L. Sala, A. Babic, H. Billich, O. Bunk, B. Schmitt, and M. Wang, JUNGFRUAU detector for brighter x-ray sources: Solutions for IT and data science challenges in macromolecular crystallography, *Struct. Dyn.* **7**, 014305 (2020).
- [18] L. Rettig, S. O. Mariager, A. Ferrer, S. Grübel, J. A. Johnson, J. Rittmann, T. Wolf, S. L. Johnson, G. Ingold, P. Beaud, and U. Staub, Ultrafast Structural Dynamics of the Fe-Pnictide Parent Compound BaFe_2As_2 , *Phys. Rev. Lett.* **114**, 067402 (2015).
- [19] D. C. Koningsberger and R. Prins, *X-Ray Absorption: Principles, Applications, Techniques of EXAFS, SEXAFS and XANES*, Chemical Analysis: A Series of Monographs on Analytical Chemistry and Its Applications, Vol. 92 (Wiley, New York, 1988).
- [20] J. Demsar, J. L. Sarrao, and A. J. Taylor, Dynamics of photoexcited quasiparticles in heavy electron compounds, *J. Phys.: Condens. Matter* **18**, R281 (2006).
- [21] J. Demsar, V. K. Thorsmolle, J. L. Sarrao, and A. J. Taylor, Photoexcited Electron Dynamics in Kondo Insulators and Heavy Fermions, *Phys. Rev. Lett.* **96**, 037401 (2006).
- [22] C. Dallera, E. Annese, J. P. Rueff, A. Palenzona, G. Vankó, L. Braicovich, A. Shukla, and M. Grioni, Determination of pressure-induced valence changes in YbAl_2 by resonant inelastic x-ray emission, *Phys. Rev. B* **68**, 245114 (2003).
- [23] A. Menth, E. Buehler, and T. H. Geballe, Magnetic and Semiconducting Properties of SmB_6 , *Phys. Rev. Lett.* **22**, 295 (1969).
- [24] N. Tsujii, H. Kontani, and K. Yoshimura, Universality in Heavy Fermion Systems With General Degeneracy, *Phys. Rev. Lett.* **94**, 057201 (2005).
- [25] M. Volkov, S. A. Sato, F. Schlaepfer, L. Kasmi, N. Hartmann, M. Lucchini, L. Gallmann, A. Rubio, and U. Keller, Attosecond screening dynamics mediated by electron localization in transition metals, *Nat. Phys.* **15**, 1145 (2019).
- [26] R. Mankowsky, A. Subedi, M. Forst, S. O. Mariager, M. Chollet, H. T. Lemke, J. S. Robinson, J. M. Glowia, M. P. Minitti, A. Frano, M. Fechner, N. A. Spaldin, T. Loew, B. Keimer, A. Georges, and A. Cavalleri, Nonlinear lattice dynamics as a basis for enhanced superconductivity in $\text{YBa}_2\text{Cu}_3\text{O}_{6.5}$, *Nature (London, U.K.)* **516**, 71 (2014).
- [27] C. Dornes, Y. Acremann, M. Savoini, M. Kubli, M. J. Neugebauer, E. Abreu, L. Huber, G. Lantz, C. A. F. Vaz, H. Lemke, E. M. Bothschafter, M. Porer, V. Esposito, L. Rettig, M. Buzzi, A. Alberca, Y. W. Windsor, P. Beaud, U. Staub, D. Zhu *et al.*, The ultrafast Einstein–de Haas effect, *Nature (London, U.K.)* **565**, 209 (2019).
- [28] J. R. L. Mardegan, S. Zerdane, G. Mancini, V. Esposito, J. R. Rouxel, R. Mankowsky, C. Svetina, N. Gurung, S. Parchenko, M. Porer *et al.*, Ultrafast electron localization in the $\text{EuNi}_2(\text{Si}_{0.21}\text{Ge}_{0.79})_2$ correlated metal, *Mater. Cloud Arch.* **2021.143** (2021), doi: 10.24435/materialscloud:5f-y0.